Curvature effects on activation speed and repolarization in an ionic model of cardiac myocytes

P. Comtois and A. Vinet
Institute of Biomedical Engineering, Université de Montréal and Research Centre, Hôpital du Sacré-Coeur, 5400 Gouin West Blvd, Montréal, Québec, Canada H4J 1C5
(Received 16 December 1998)

Reentry is a major mechanism underlying the initiation and perpetuation of many cardiac arrhythmias [1–5]. Stimulated ventricular myocytes give action potential characterized by a fast upstroke, a long-lasting plateau, and a late repolarization phase. The plateau phase determines the action potential duration (APD) during which the system remains refractory, a property essential to the synchronization of the heart cycle. The APD varies much with prematurity and this change has been shown to be the main determinant of the dynamics in models of paced cells and cable, and during reentry in the one-dimensional loop. Curvature has also been shown to be an important factor for propagation in experimental and theoretical cardiac extended tissue. The objective of this paper is to combine both curvature and prematurity effects in a kinematical model of propagation in cardiac tissue. First, an approximation of the ionic model is used to obtain the effects of curvature and prematurity on the speed of propagation, the APD, and the absolute refractory period. Two versions of the ionic model are studied that differ in their rate of excitability recovery. The functions are used in a kinematical model describing the propagation of period-1 solutions around an annulus. [S1063-651X(99)07310-9]

PACS number(s): 87.19.Hh, 05.45.−a

I. INTRODUCTION

Reentry is a major mechanism underlying the initiation and perpetuation of many cardiac arrhythmias. Transient or sustained propagation has been shown to occur around an anatomical obstacle, or around a region of partially or totally unexcitable tissue [1–3]. Sustained activation fronts with the form of vortices have been observed in healthy substratum [4,5]. A large amount of modeling work has also been devoted to reentry, with approaches ranging from cellular automata to systems of partial differential equations involving high-dimensional ionic models [6–9]. This paper is focused on reentry in an homogeneous two-dimensional annulus of ventricular excitable tissue with a central hole.

Stimulated ventricular myocytes produce action potential characterized by a fast upstroke, a long-lasting plateau, and a late repolarization phase. The plateau phase determines the action potential duration (APD) during which the system remains refractory, a property essential to the synchronization of the heart cycle. The APD varies extensively with prematurity and this change has been shown to be the main determinant of the entrainment response in a model of paced cells and paced cable, and of the regimes of reentry in a one-dimensional loop [10–17]. In ionic models, the plateau phase requires the inclusion of at least one additional inward current acting on an intermediate time scale between the fast activating current of the upstroke and the slow current of repolarization that makes the difference between nerve cell and cardiac cell models. We used a modified Beeler-Reuter (MBR) model of the cardiac myocyte, which is the simplest ionic model meeting this requirement. We also used this model because its dynamics have been thoroughly studied in the space-clamped, cable, and loop configurations. In these settings, the main features of the dynamics of the MBR model have been reproduced by simple nonlinear low-dimensional models [14,16,17]. Our purpose is to extend these simple models to the annulus.

Curvature has been shown to be a determinant of propagation both in the experimental and the theoretical model of cardiac extended tissue [18–21]. Zykov has developed a kinematical model with a linear dependence between velocity and curvature [22] that is not accurate in the presence of dispersion. The kinematical model was extended [23,24] to include the effect of rate-dependent change of velocity, and stability analysis has shown that perturbations of curvature near the core may destabilize the solution [25,26]. Other simple representations were proposed using singular perturbation methods on Fitzhugh-Nagumo-type (FHN) models [27–30], and an eikonal relationship was developed using a finite renormalization method [31,32]. The APD restitution was not considered in these works.

The objective of this paper is to combine both curvature and prematurity effects in a kinematical model of propagation in cardiac tissue. First, an approximation of the ionic model is used to obtain the effects of curvature and prematurity on the speed of propagation, the APD, and the absolute refractory period. Functions are obtained to describe these quantities. Two versions of the ionic model are studied that differ in their rate of excitability recovery. The functions are used in a kinematical model describing the propagation of period-1 solutions around an annulus that is solved numerically. The influence of prematurity and curvature on the form and stability of the solutions is discussed.

II. METHODS

A. Model

The well-known cable equation in a two-dimensional (2D) homogeneous isotropic excitable cardiac medium embedded in an unbounded external medium of negligible resistivity is

$$\frac{1}{\rho}\vec{\nabla}\cdot\vec{\nabla}V = S\left(C_M\frac{\partial V}{\partial t} + I_{ion}\right), \tag{2.1}$$

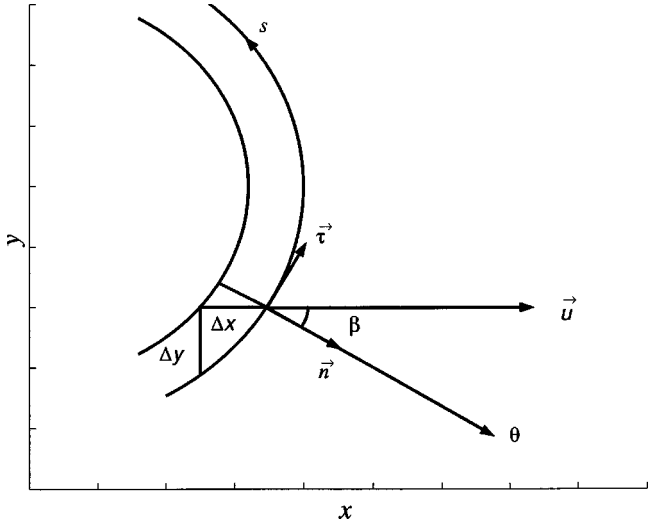

FIG. 1. Schematic representation of a wave propagating with a local curvature *K*. $\vec{u}$ is the speed in the direction of propagation of the front, θ the speed of propagation perpendicular to the isoline (parallel to the unit vector $\vec{n}$), β the angle between the real speed $\vec{u}$ and $\theta\vec{n}$, $\vec{\tau}$ the unit vector parallel to the isoline, and *s* the curvilinear coordinate of the isoline.

where V is the transmembrane potential (mV), C_M is the membrane capacitance ($1\mu\mathrm{F\ cm^{-2}}$), S the surface-to-volume ratio ($0.4\ \mu\mathrm{m^{-1}}$, assuming cylindrical cells with a radius of 5 μm), and ρ is the mean intracellular resistivity (200 Ω cm). The membrane ionic model used to calculate I_{ion} is a modification of the Beeler-Reuter model of the ventricular myocyte cell membrane [33].

The gating variables y_i of the MBR model are governed by a first-order process described by a steady-state value $y_{i\infty}(V)$ and a time constant $\tau_{y_i}(V)$. The total ionic current is the sum of a fast sodium current I_{Na}, a secondary inward current I_{si} assumed to be carried mainly by calcium ions, a delayed outward potassium current I_K, and a time-independent potassium current I_{K1}. Here, $I_{Na}=\bar{g}_{Na}m^3hj(V-E_{Na})$, where $\bar{g}_{Na}=15\ \mathrm{ms\ cm^{-2}}$ is the maximum conductance; $E_{Na}=40$ mV is the sodium equilibrium potential; and m, h, and j are the gating variables. $I_{si}=\bar{g}_{si}df(V-E_{si}([\mathrm{Ca}]))$, where $g_{si}=0.09\ \mathrm{ms\ cm^{-2}}$ is the maximum conductance, $E_{si}([\mathrm{Ca}])$ is a calcium-dependent reversal potential, and d and f are the gating variables; in this model, $I_K=I_{K1}+x_1I_{x1}$ is governed by a gating activation variable $x1$ and a fixed equilibrium potential $E_K=-94$ mV, and I_{K1} is an empirical function. To study the effect of slower [Na] channel recovery, simulations where done with the nominal τ_j (normal model) and with τ_j increased by a factor of 6 (slow model).

Figure 1 shows an isopotential $\bar{V}$ in Cartesian coordinates at times t and $t+\Delta t$. In the new coordinates defined by the unit vectors $\vec{n}$ and $\vec{\tau}$ in the direction normal and tangent to the equipotential and the associated coordinates z and w, Eq. (2.1) becomes [22]

$$\frac{1}{\rho S}\left(\frac{\partial^2 V}{\partial z^2}+\frac{\partial\beta}{\partial s}\frac{\partial V}{\partial z}+\frac{\partial^2 V}{\partial w^2}\right)=C_M\frac{\partial V}{\partial t}+I_{ion}. \qquad (2.2)$$

Since $\vec{n}$ coincides with the direction of $\vec{\nabla}V$, the gradient along $\vec{\tau}$ is null, so that $\partial^2V(z,w,t)/\partial w^2=0$. The term $\partial\beta/\partial s$ is equal to the curvature $K(s)$ of the equipotential. For a circular front propagating from the middle of a circular medium, the correspondence is $K=1/r$ and $z=r$. If K is taken as constant, Eq. (2.2) becomes a one-dimensional system that represents the propagation of a waveform with a constant arbitrary curvature. This approximation was used to study the effect of curvature on the speed of propagation and on the repolarization. The sign of curvature K is positive for a convex front due to the vector convention used in the development.

Equation (2.2) was simulated for a finite medium $z=[0,L]$ with no flux boundary conditions. L was set to 10 cm (2000 nodes). The system was first discretized in time with a constant time step ($\Delta t=0.002$ ms) and I_{ion} was solved with an hybrid method described in [34,35]. For each time step, the system becomes a second-order ordinary differential equation, which was approximated with a Galerkin finite element method projected on a linear basis function (*hat function*) and a regular spatial mesh ($\Delta z=0.005$ cm) [36]. The resulting tridiagonal linear system of equations was solved with a simplified LU decomposition method. The choice of Δt and Δz is motivated by the fact that depolarization is the stiffest part of the process. Programs were written in C and run on an SGI workstation (Silicon Graphics).

B. Simulations

Simulations were performed for different values of the parameter K with normal and slow τ_j. Starting with the system at its resting state and a given value of K, propagation was initiated by applying for $t_{st}=1$ ms a stimulation of $I_{st}=100\ \mu\mathrm{A/cm^2}$ on 40 nodes starting at $L=0$. During propagation, the beginning of the action potential (AP) at each node (t_{dep}) was taken as the instant at which dV/dz reaches its maximum. The end of the action potential (t_{rep}) was defined as the time at which V crosses -50 mV during repolarization. The speed of propagation $\theta_\infty(K)$ was calculated from the difference of t_{dep} between points spaced by ten nodes to reduce discretization error. The APD at each node was calculated as the difference between t_{rep} and t_{dep}. Propagation was also initiated by applying premature stimulations at various times after the onset of the first AP. The diastolic interval (DI) was then defined at each node as the time from the end of the test AP to the beginning of the next AP. Expressions were developed to represent the variation of θ and APD as functions of K and DI. Results of simulation were fitted using a least-squares minimization procedure of Matlab (Mathworks Inc., MA).

III. RESULTS

A. Velocity and *A* from rest

To evaluate the effects of curvature on velocity and APD from rest, measurements were averaged over a set of 50 nodes in the middle of the media (i.e., 5 cm from the simulation site). This was done to overcome the effects of boundaries. Simulations have shown an increase of velocity for a distance less than 0.07 cm near both ends of the media for all K values.

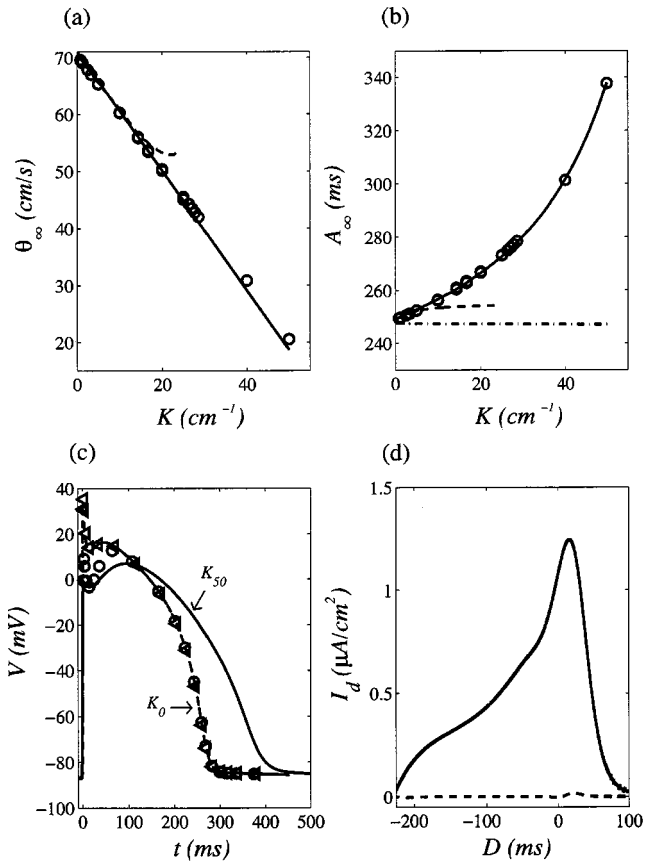

FIG. 2. (a) $\theta_\infty(K)$ calculated with Eq. (2.2) assuming constant curvature ($\bigcirc$) and fitted by Eq. (3.1) (full curve). The dashed curve is $\theta_\infty(K)$ for a propagating target pattern. (b) $A_\infty(K)$ calculated for a front with fixed curvature ($\bigcirc$) and fitted by Eq. (3.2) (full curve). The dash-dot curve indicates the value for a plane wave ($K=0$) and the dashed curve those obtained for a propagating target pattern. (c) The AP at the central node for a plane wave (K_0, dashed curve) and a front with $K=K_{cr}=50\ \mathrm{cm}^{-1}$ (K_{50}, full curve). Space-clamped AP with initial conditions taken at V_{max} of the plane wave ($\triangle$) and the wave with $K=K_{cr}$ ($\bigcirc$). (d) Diffusion current (I_d) for the plane wave (dashed curve) and the wave with $K=K_{cr}$ (full curve).

As the curvature of the propagation front increases, the ratio of the surface to depolarize to the excited surface increases, inducing a slowing of the propagation. It is widely accepted that the linear expression,

$$\theta_\infty(K)=\theta_0-\mu K, \quad \mu>0, \tag{3.1}$$

where K is the curvature, θ_0 the speed of the plane wave, and μ a hybrid diffusion coefficient, gives a good approximation of propagation velocity as a function of the curvature in an excitable media at equilibrium [22,32]. Figure 2(a) shows that Eq. (3.1), with $\theta_0=70.29\ \mathrm{cm\ s}^{-1}$ and $\mu=1.05\ \mathrm{cm}^2\ \mathrm{s}^{-1}$, fits the values of $\theta_\infty(K)$ obtained by simulation. Results found with both nominal and slow $\tau_j(V)$ are superimposed since j deactivates after the upstroke and has no influence on the speed from rest. Equation (3.1) holds for convex ($K>0$) as well as concave ($K<0$) fronts. Sustained propagation was found until $K_{cr}=50\ \mathrm{cm}^{-1}$. For $K>K_{cr}$, the propagating AP was vanishing within a distance of 200 nodes.

These results were also compared with those of Eq. (2.2) with the modifications corresponding to the propagation of a circular target wavefront [dashed curve in Fig. 2(a)]. Stimulation was applied on the first ten nodes of the medium ($r=0.05$ cm, $K=20\ \mathrm{cm}^{-1}$). In this case, the curvature changes continuously as propagation proceeds. Nevertheless, results of both models stay close to $K=15\ \mathrm{cm}^{-1}$. Near the center, the transient associated with the stimulation, the accumulation of current due to the symmetry condition, as well as the steep change of curvature mask the relation between speed and curvature. We have also constructed a curve of the threshold current as a function of the radius of stimulation. We found that 0.012 cm was the smallest radius to induce a sustained propagation. $r_{stim,min}$ (0.012 cm) is less than $1/K_{cr}$ (0.020 cm), but the difference is much below the distance over which transient propagation was found for the front with constant $K>K_{crit}$.

In repolarization, the ratio of depolarized to repolarized surface is the inverse of what exists at the fringe of the excitation front. The term $K\partial V(z,w,t)/\partial z$ in Eq. (2.2) is positive, such that the APD is prolonged, as shown in Fig. 2(b). Again, results with normal and slow $\tau_j(V)$ functions are superimposed. The variation of APD with K ($A_\infty(K)$) is important, since the APD increases from 249.15 ms for a plane wave ($K=0$, dash-dot curve) to 337.35 ms at the critical curvature, a variation of more than 35% in duration. The relation between APD and K can be fitted within a 1% error by the exponential function [full curve in Fig. 2(b)]

$$A_\infty(K)=A_0 e^{-1/[\tau(K-a_1)]}, \tag{3.2}$$

with $A_0=200.31$ ms, $a_1=86.07\ \mathrm{cm}^{-1}$, and $\tau=0.053$ cm. Again the target circular wavefront (dashed curve) gives similar results at low curvature. However, the increase is stopped due to the symmetry and stimulation effects at the center.

Figure 2(c) shows the action potential at one node for $K=0$ (plane wave, dashed curve) and $K=50\ \mathrm{cm}^{-1}$ (full curve). The APD at critical curvature is clearly longer, but it is also associated with lower V_{max} at the upstroke. To find if the prolongation of the APD was induced by the difference of upstroke, we took the state of all variables at the time of V_{max} as the initial condition for simulations of the space-clamped model. The space-clamped action potentials given by initial conditions taken from the plane wave ($\triangle$) and the critical curvature ($\bigcirc$) come together and follow the same time course as the action potential of the propagated plane wave. The same procedure was repeated for all curvatures, and the same APD was obtained for all cases. As shown in Fig. 2(d), the prolongation of the APD at high curvature is caused by the increase of the diffusion current, which peaks around $D=0$ during repolarization.

B. Refractory period and $D_{min}(K)$

After an upstroke, the slow gate variables h and j of I_{Na} deactivate, and propagation is impossible until recovery of a minimal level of excitability. The minimum DI (D_{min}) is the minimal time after which a second activation front can be initiated. In general, it depends both on the parameters of the stimulation and on the nature of the action potential after which the stimulus is applied. After a first stimulation from

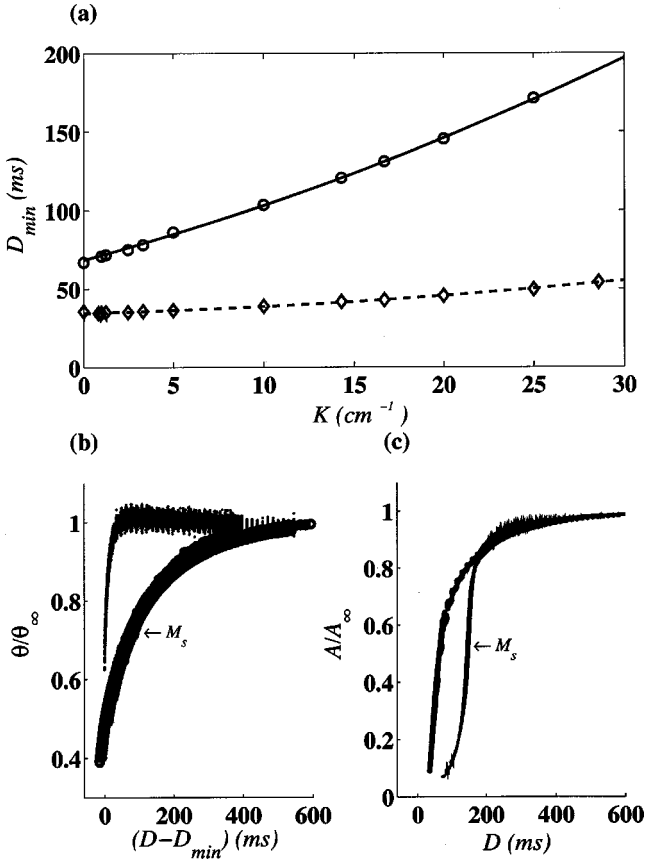

FIG. 3. (a) $D_{min}(K)$ for the normal ($\diamond$) and slow ($\bigcirc$) models. Full curves are the fits by Eq. (3.3). (b) $\theta(D,K)/\theta_\infty$ vs $D-D_{min}(K)$ for the normal and slow models (M_s) and (c) $A(K,D)/A_\infty(K)$ for the normal and M_s models.

rest, the same stimulus was applied at various prematurity to find $D_{min}(K)$, the variation of the D_{min} with K. Figure 3(a) shows the results for the normal ($\diamond$) and slow ($\bigcirc$) model. As expected, slower recovery for j prolongs the D_{min}. As K increases, more current is also needed to sustain propagation, so that the D_{min} increases. The effect is much more important for the slow model. $D_{min}(K)$ was fitted with the second-order polynomial

$$D_{min}(K)=d_0+d_1K+d_2K^2, \tag{3.3}$$

with $[d_0,d_1,d_2]$ equal to [34.6,0.29,0.013] and [68.5,3.07,0.04] for the normal and slow models, respectively.

C. Velocity $\theta(K,D)$ and AP duration $A(K,D)$: General representations

Results of premature stimulations were used to obtain $\theta(K,D)$ for each value of K. The propagation velocity is a function of both D and K. However, as shown in Fig. 3(b), plotting $\theta(K,D)/\theta_\infty(K)$ as a function of $D-D_{min}(K)$, where D stands for the DI, produces curves that are independent of K for both the slow and normal models. For the normal model, there is a steep increase of $\theta(K,D)/\theta_\infty(K)$ in a small interval near $D_{min}(K)$, while the variation is much more progressive for the slow model. Both curves were fitted with the double exponential function,

$$\theta(K,D)=\theta_\infty(K)f_\theta(D-D_{min}(K)), \tag{3.4}$$

$$f_\theta(y)=(1-B_1e^{-y/\tau_1}-B_2e^{-y/\tau_2}),$$

where $\theta_\infty(K)$ and $D_{min}(K)$ are given by Eqs. (3.1) and (3.3), and $[B_1,B_2,\tau_1,\tau_2]$ take the values [0.205,0.300,19.0,3.54] for the normal model and [0.420,0.084,135.7,338.6] for the slow model. In summary, D_{min} increases with K and $\theta_\infty(K)$ diminishes, but $\theta(K,D)/\theta_\infty(K)$ can be expressed as an invariant function of $D-D_{min}(K)$. This shows that the DI is more appropriate than the period of rotation [31] to express the change of velocity as a function of prematurity.

$A(K,D)$ were obtained by the same protocol used for $\theta(K,D)$. Figure 3(c) shows that $A(K,D)/A_\infty(K)$ plotted as function of D defines invariant curves for the normal and slow models. For the normal model, $A(K,D)/A_\infty(K)$ varies as a double exponential function with a steep initial increase, followed by a slow drift toward the saturation value. In the slow model, the initial phase has a sigmoid appearance, but tends toward the same saturation value and its variation comes at higher DI. Thus, delaying the recovery of I_{Na} excitability increases D_{min} and extends the DI interval with low APD values. The curves were fitted with the relation

$$A(K,D)=A_\infty(K)F(D), \tag{3.5}$$

$$F(D)=\left\{1-a_l+B(D)\frac{D}{w^v+D}-l_2e^{-D/\tau_2}\right\},$$

$$B(D)=a_l-l_1e^{-D/\tau_1},$$

with the same $A_\infty(K)$ [Eq. (3.2)] for both models and $[a_l,l_1,\tau_1,w,v,l_2,\tau_2]$ equal to [0,3.9,29.2,1,0,0.45,166.9] for the normal model and [0.66,0.13,278.7,143.9,17.6,0.62,94.1] for the slow model.

D. Clue to stability

The stability of MBR-type models has been analyzed for the isolated cell and the one-dimensional cable and loop [14,15,17,35]. In all cases, results of the ionic models were shown to be largely reproduced by low-dimensional models using the DI as an independent variable. In these low-dimensional models, period-1 responses occur when $D+A(D)=T$, where T is either the constant stimulation period (paced membrane and cable) or the period of circulation (reentry on loop). For cable and loop, the equality holds for all points in the medium. The stability of the period-1 solution is lost at the T corresponding to the critical DI value where

$$\left|\frac{dA}{dD}\right|_{D_{crit}}=1. \tag{3.6}$$

Consider the stable rotation of an activation front in an isotropic and homogeneous annulus with internal and external radius r_{in} and r_{out} and no flux boundary conditions. The activation front is a curve extending from r_{in} to r_{out} that rotates with a fixed period T. The propagation velocity $\theta(K,D)$ is everywhere normal to the front. At r_{in}, the no-flux boundary condition constrains θ to be tangent to the circumference. Zykov [22] has shown that the curvature

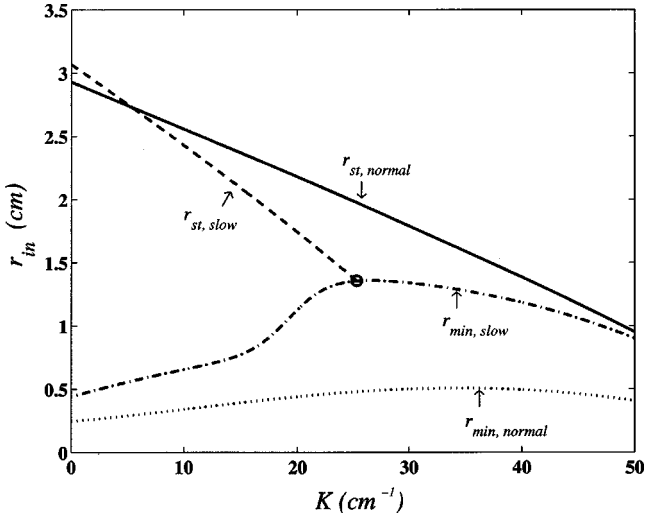

FIG. 4. r_{min} [Eq. (3.9)] and r_{st} [Eq. (3.10)] as a function of K for the normal (dotted and full curves) and the slow (dash-dot and dashed curves) models.

must be maximum at r_{in}. As a first approximation, assume also that the curvatures of activation and repolarization fronts are the same. Then, at r_{in}, the relation

$$T=\frac{2\pi r_{in}}{\theta(K,D)}=D+A(K,D) \tag{3.7}$$

must be satisfied.

At $D_{min}(K)$, the minimum value at which propagation can be sustained, Eq. (3.7) becomes

$$r_{min}(K)=\frac{\theta(K,D_{min}(K))[D_{min}(K)+A(K,D_{min}(K))]}{2\pi} \tag{3.8}$$

and, by Eq. (3.4),

$$r_{min}(K)=\frac{\theta_{\infty}(K)f_{\theta}(0)[D_{min}(K)+A(K,D_{min}(K))]}{2\pi}. \tag{3.9}$$

So $r_{min}(K)$, the minimum radius for propagation with curvature K, depends on the opposite effects of $\theta_{\infty}(K)$, which decreases with K, and on $D_{min}(K)+A(K,D_{min}(K))$, which increases. $r_{min}(K)$ for the nominal (dotted curve) and slow (dash-dot) models are shown in Fig. 4. At low K, the increase of $D_{min}(K)+A(D_{min}(K))$ is dominant, and r_{min} grows.

The balance is reversed at high K. The effect is much more pronounced for the slow model because the increase of D_{min} with K is more important [Fig. 3(a)]. Slowing τ_j was done to reflect in a crude fashion the fact that class-IA drugs are known to delay the recovery of excitability [37,38]. It thus increases $r_{min}(K)$. Equation (3.9) provides a lower estimate for $r_{min}(K)$, since it is supposed that propagation can be sustained with $D=D_{min}(K)$ constant along the circumference of the annulus. This is not the case in a ring for which the stability criterion is given by Eq. (3.6).

If we accept that the same criterion applied to the annulus, then $D_{crit}(K)$ corresponds to the value for which $\partial A(K,D)/\partial D=1$. If it is larger than $D_{min}(K)$, it is the smallest DI value to get a stable period-1 circulation. We define $D_{st}(K)$ as

$$D_{st}(K)=\begin{cases} D_{crit}(K) & \text{if } D_{crit}(K)>D_{min}(K), \\ D_{min}(K) & \text{if } D_{crit}(K)\leqslant D_{min}(K). \end{cases} \tag{3.10}$$

In the slow model, there are two values of D_{crit} because of the sigmoidal form of $A(K,D)$ [Fig. 3(b)]. The upper value was kept for calculation. The insertion of D_{st} in Eq. (3.8) gives, with $y=D_{st}(K)-D_{min}(K)$,

$$r_{st}(K)=\frac{\theta_{\infty}(K)f_{\theta}(y)[D_{st}(K)+A(K,D_{st}(K))]}{2\pi}. \tag{3.11}$$

$r_{st}(K)$ is shown in Fig. 4 for the normal model (full curve) and the slow model (dashed curve). For the normal model, $D_{st}=D_{crit}$ for all K, while for the slow model, there is a maximum K value from which $D_{st}(K)=D_{min}(K)$ and $r_{st}(K)=r_{min}(K)$.

When K is low, $D_{st}=D_{crit}$ for both models. Since the value of D_{crit} does not vary much with K, the decrease of $r_{crit}(K)$ is controlled by the drop of $\theta_{\infty}(K)$ and $f_{\theta}(D_{st}(K)-D_{min}(K))$. In the normal model, D_{min} is almost constant, but it increases rapidly in the slow model [Fig. 3(b)], which explains why $r_{crit}(K)$ has a higher slope.

If the criterion of stability is valid, the area over $r_{st}(K)$ corresponds to stable period-1 circulation, and propagation may be sustained but not period-1 for $[r,K]$ values between $r_{st}(K)$ and $r_{min}(K)$. At low K, r_{st} is larger for the slow model, because D_{crit} is larger (200 ms vs 170 ms at $K=0$). At higher curvature, the lower velocity of the slow model compensates for the difference in D_{crit}, and the slow model has a lower r_{st}. For $K<5.4\ \text{cm}^{-1}$, both r_{st} and r_{min} are larger in the slow model. Beyond $K=5.4$, slowing τ_j decreases the minimal radius for stable propagation but reduces the possibility of non-period-1 reentry.

E. Reentry in an annulus

The stability of propagation also depends on the additional constraints imposed by the spatial extension of the front throughout the annulus. Different kinematic descriptions of propagation in two-dimensional (2D) excitable media have been proposed [22,29,32,39,40]. Zykov [22] has considered the activation front as a continuous line and described the change of velocity along a stable rotating front as

$$\frac{d\theta}{ds}=\omega-Kv=f_1,$$

$$\frac{dv}{ds}=K\theta=f_2, \tag{3.12}$$

where ω is the angular velocity. θ, v, and K are, respectively, the speed normal and parallel to the front, and the curvature, which are functions of s, the curvilinear coordinate along the front. In an annulus with no flux boundary conditions at the inner (r_{in}) and outer (r_{out}) radii, the solution must satisfy the constraints

$$v=0 \quad \text{at } r_{in} \text{ and } r_{out}. \tag{3.13}$$

Since θ and v are functions of K and D, each point along the front is also characterized by a value $D(s)$ that satisfies the additional constraint

$$\frac{2\pi}{\omega}=D(s)+A(D(s),K(s)). \tag{3.14}$$

Assuming that the curvatures at the excitation front and the repolarization front are the same, then

$$\frac{dD}{ds}=-\frac{dA}{ds},$$

$$\frac{d\theta}{ds}=\frac{\partial\theta}{\partial K}\frac{dK}{ds}+\frac{\partial\theta}{\partial D}\frac{dD}{ds}, \tag{3.15}$$

$$\frac{dA}{ds}=\frac{\partial A}{\partial K}\frac{dK}{ds}+\frac{\partial A}{\partial D}\frac{dD}{ds}.$$

Putting together Eqs. (3.12) and (3.15) and using the notation $y_x=\partial y/\partial x$ for partial derivatives, the final system is given by

$$\frac{dD}{ds}=\frac{f_1}{A_1},$$

$$\frac{dK}{ds}=\frac{f_1}{\theta_K}\left(1-\frac{\theta_D}{h_1}\right), \tag{3.16}$$

$$\frac{dv}{ds}=f_2,$$

$$\text{with } h_1=\theta_D-\frac{\theta_K}{A_K}(A_D+1).$$

The system must be solved between r_{in} and r_{out} with the constraints (3.13) and (3.14). As stated in Sec. III D, at r_{in}, the constraints imply that

$$D=\frac{2\pi r_{in}}{\theta(K,D)}-A(K,D) \tag{3.17}$$

$$=g(K,D)\geqslant D_{min}(K)$$

which defines an implicit relation between K and D. For each K, $\partial g(K,D)/\partial D<0$, such that Eq. (3.17) has either one or no solution, i.e., the number of solution (N) is given by

$$N\rightarrow\begin{cases}1 & \text{if } g(K,D_{min}(K))\geqslant D_{min}(K)\\ 0 & \text{if } g(K,D_{min}(K))<D_{min}(K).\end{cases}$$

The system (3.16) can be solved numerically for a given r_{in} with a method similar to the one described by Zykov in [22]. To do so, a value of K is chosen at r_{in} and Eq. (3.17) is solved by a Matlab minimization procedure (MathWorks, Inc.). If the solution exists for D, it provides the value of ω by Eq. (3.14) and an initial condition of Eq. (3.16). The system is then integrated using Rosenbrock's stiff integrator of the Matlab ordinary diffential equation (ODE) suite [41]. The trajectory in the $[D,K,v]$ space is an acceptable solution

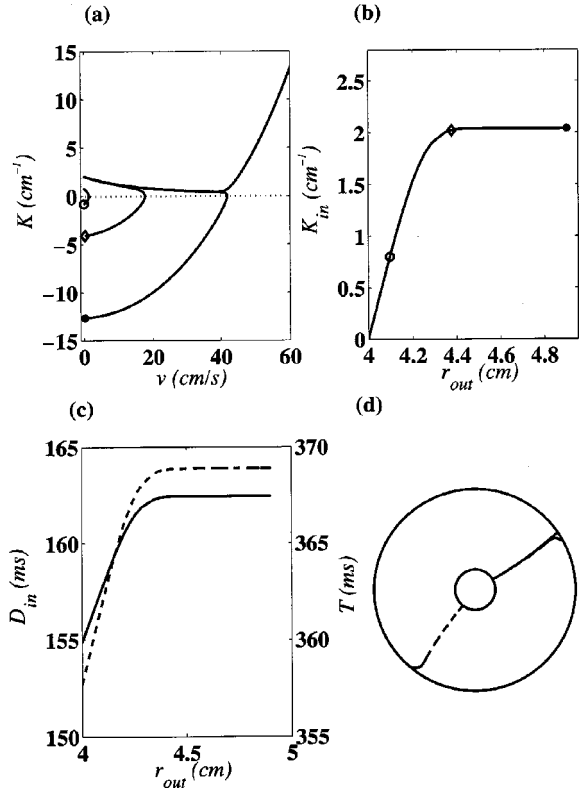

FIG. 5. (a) Solutions of Eq. (3.16) in the (v,K) plane for four different initial conditions (IC) K_{in} in the case $r_{in}=4$ cm for the normal model. ○, ◇, and ● correspond to the final state at r_{out} for the K_{in} IC shown in panel (b). The upper trajectory which is not an acceptable solution, was obtained using the (○) IC K_{in} plus 10^{-13} cm^{-1}. (b) K_{in} vs r_{out} for acceptable solutions. (c) T (full curve, right ordinate) and D_{in} (dashed curve, left ordinate) vs r_{out}. (d) The form of the solution in space for $r_{out}=4.95$ cm. The plot was rescaled with $r_{in}=0.5$ cm and $r_{out}=2.5$ cm to improve the viewing. The depolarization (full curve) and the repolarization (dashed curve) fronts are shown. After rotation, the two fronts are superimposed.

if $K(s)\leqslant K_{crit}=50$ cm^{-1} and $D(s)\geqslant D_{min}(K(s))$. It ends at the point where $v(s)=0$, which corresponds to the constraint at r_{out}.

Figure 5(a) shows the projection in the $[v,K]$ plane of the trajectories obtained for the normal model with $r_{in}=4$ cm and different K at r_{in} (K_{in}). The limit case for acceptable solutions is the trajectory for which v converges asymptotically toward $K=0$. It corresponds to propagation in an infinite medium ($r_{out}\rightarrow\infty$). Trajectories above this curve are not solutions. Because K is always maximum at r_{min}, the period of rotation must decrease as a function of r_{out} [Fig. 5(c), full curve]. There are two ways to decrease the speed at r_{in}: increasing K or decreasing D. However, D cannot be diminished because it is constrained by the relation (3.14) [Fig. 5(c), dashed curve]. Hence, K_{in} must increase as a function of r_{out} [Fig. 5(b)]. The rise of K_{in} saturates for $r_{out}\approx 4.5$ cm. Indeed, when $r_{out}-r_{in}>0.5$ cm, K_{in} is as it is in an infinite medium.

Figure 5(d) shows the form of the activation (full curve) and repolarization front (dashed curve) in space for $r_{out}=4.95$ cm. It corresponds to the lower trajectory in panel (a). The ODE solver provides a discretized approximation of the

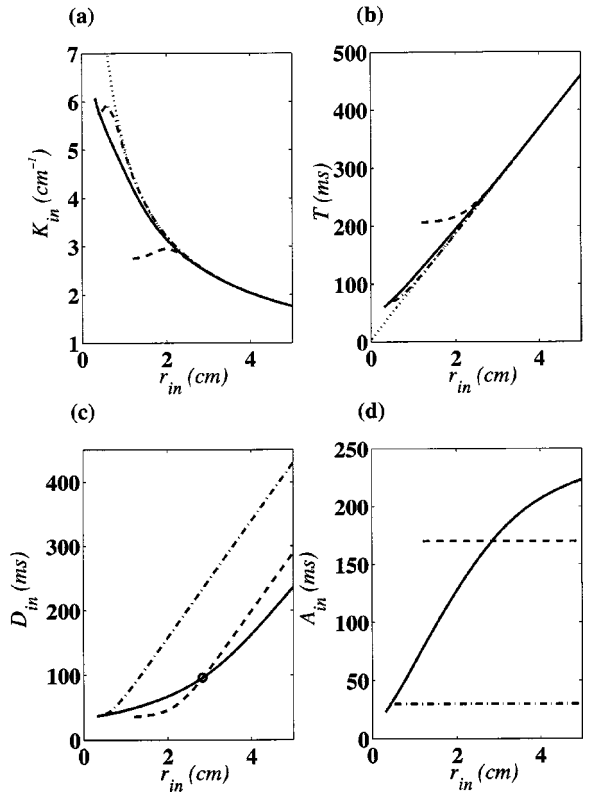

FIG. 6. Characteristics of the propagating wave in an unbounded ring as a function of r_{in} from Eq. (3.16) with the functions derived from the normal model. Four variants of the low-dimensional model, which included the complete model (full curve), $\theta(K,D)$ and $A=200$ ms (dashed curve), $A=30$ ms (dash-dot curve), and $\theta_\infty(K)$ only (dotted curve). The case with $\theta(K,D)$ and $A(0,D)$ is superimposed on the complete model: (a) curvature at the inner boundary K_{in}, (b) period of rotation, (c) diastolic interval DI at r_{in}, and (d) APD at r_{in}.

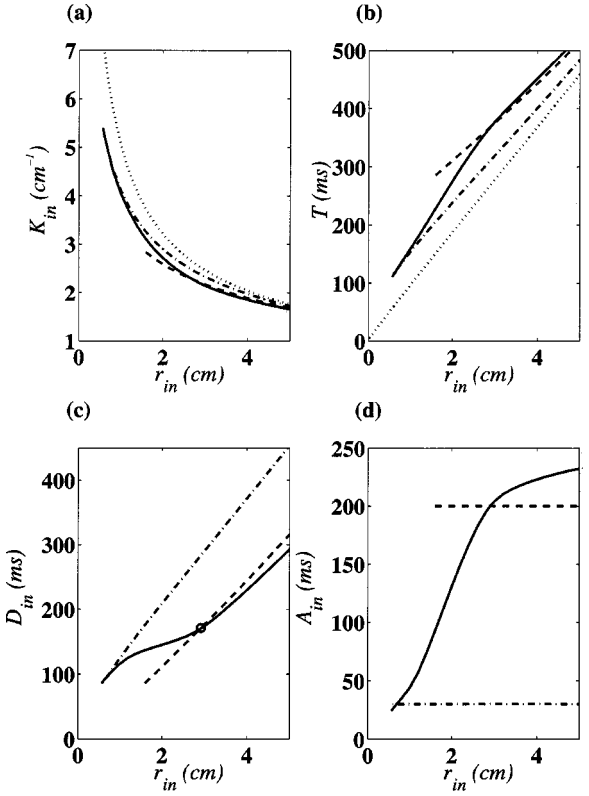

FIG. 7. Same as Fig. 6 for the functions coming from the slow model. The dashed curves are obtained with $A=170$ ms.

trajectory by the set of points $\{s_i,\theta_i,K_i,D_i,i=1,2,\ldots,n\}$. First $r(s_i)=r_i$ is computed using the relation $\omega^2 r_i^2=v_i^2+\theta_i^2$ [Eq. (6.23) in [22]]. Then the increment in ϕ $(\Delta\phi)$ between r_i and r_{i+1} is calculated by triangulation, assuming that $s_{i+1}-s_i$ can be approximated as a straight line. The approximation is justified, since the maximum $\Delta\phi$ is of the order of 10^{-5} rad. The repolarization front was defined as the set of points with $D=0$. The figure was scaled (see caption) to get a clearer picture of the fronts. The portion of the front with $K<0$ corresponds to a tiny segment near r_{out}. After rotation, the repolarization front is superimposed almost everywhere on the activation front, such that the hypothesis of equal curvature used in Eqs. (3.16) for the two fronts is fulfilled.

Solutions were computed as a function of r_{in} for an infinite medium ($r_{out}\to\infty$) for both the normal (Fig. 6) and slow models (Fig. 7). To delineate the effect of K and D on the solutions, simulations were done with:

(i) $\theta_\infty(K)$ only (dotted curve).

(ii) $\theta(K,D)$ and APD constant fixed at $A(D_{st})$ as defined in Eq. (3.10) (normal, 170 ms; slow, 200 ms; dashed curve) or 30 ms (dash-dot curve).

(iii) $\theta(K,D)$ and $A(0,D)$.

(iv) $\theta(K,D)$ and $A(K,D)$ (full curve).

The curves for cases (iii) and (iv) are superimposed, meaning that the modulation of APD by K has minimal influence on the solutions because K never becomes high enough [panel (a)] for the correction to be important [see $A_\infty(K)$ in Fig. 2]. It means that, for each r_{in}, DI and APD can be considered constant in space and the activation and repolarization fronts have the same curvature. Case (ii), with $A=A(0,D_{crit})$, gives a much too high minimal value for r_{in} [panel (a), dashed curve], but comes closer to the complete model value for $A=30$ ms (dash-dot curve). This can be understood by comparing the range of APD covered by the complete model to the fixed levels used for calculation [panel (d)]. Since $A=30$ ms is close to the minimum APD reached for both models, its allows a good approximation of D_{min} [panel (c)], of the period rotation T at low r_{in} [panel (b)], and hence of the minimal r_{in}. However, APD is a fast increasing function of r_{in}, such that using a fixed APD gives a poor reproduction of D_{in} as a function of r_{in} [panel (c)]. D_{in} increases too rapidly, as well as T [panel (b)], since θ is also an increasing function of D. The difference in the period of rotation is more important for the slow model, for which the effect on D and θ is more pronounced. In summary, $\theta(K,D)$ and $A(D)$ are needed for a good representation of the dynamics, but the effect of K on APD can be neglected. This is emphasized by the comparison of the complete model with case (i) (dotted curve), which included only $\theta_\infty(K)$. Because the slowing of propagation at low DI is lacking, the curvature of case (i) is larger. Besides, the main factor fixing the minimum r_{in} (0.33 cm, normal model; 0.578 cm, slow model) in the complete model is $D_{min}(K)$, whose calculation requires $A(D)$. For case (i), the minimum r_{in} is fixed only by K_{cr}, giving a much too short minimal r_{in} ($1/K_{cr}=0.02$ cm

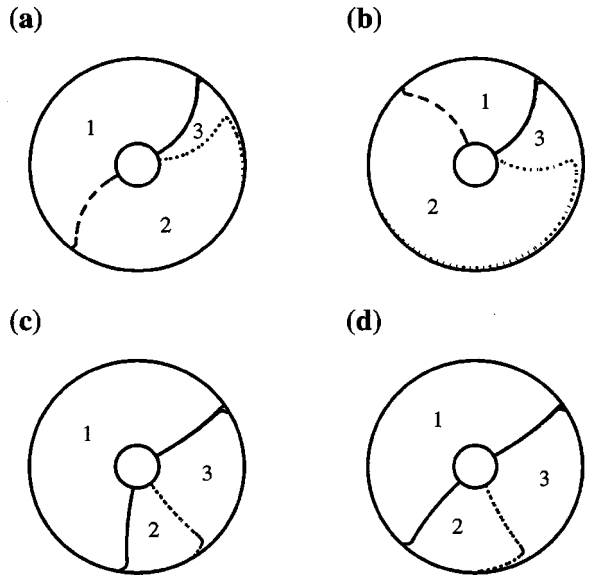

FIG. 8. Depolarization (full curve), repolarization (dashed curve), and D_{min} (dotted curve) fronts for the normal (a),(c) and slow model (b),(d) for $r_{in}=0.6$ cm (top row) and $r_{in}=r_{crit}$ (bottom row). These curves separate the domain into three distinct regions: 1, AP; 2, refractory period (RP); and 3, excitable gap (EG).

vs 0.33 cm and 0.578 cm for the normal and slow models).

The stability of the above solutions remains to be established. As an indication, the (○) in panel (c) of Figs. 6 and 7 shows the value of r_{in} where D_{in} is equal to D_{st}. It is higher for the slow model. Since K at r_{crit} is below 5.4 cm^{-1}, this agrees with the prediction made in Sec. III D.

Finally, Fig. 8 shows the form of the solutions with $r_{in}=r_{crit}$ (bottom row) and 0.6 cm, which is closed to r_{min} for the slow model (top row). r_{out} was taken 1 cm larger than r_{in}, beyond the range where its variation may influence the solution around r_{in}. Solutions are shown for the normal (left column) and slow (right column) model. The full curve is the activation front, and the dashed curve, the repolarization front. After rotation, the two fronts are superimposed, except near r_{out} where the high negative curvature imposed by the boundary condition induced a noticeable reduction of the A. The dotted curve is the locus of the points with $D=D_{min}(K)$. Region 1 encloses all the points where the action potential is not finished; regions 2, the points that are still in their refractory period. Region 3 corresponds to the excitable gap, in which a new action potential could propagate. For both r_{in}, the slow model has a smaller region 1 (smaller A), longer region 2 [longer $D_{min}(K)$], resulting in a larger excitable gap (EG) (region 3). Moving from the center to the periphery, K and D_{min} decrease, such that the EG enlarges. Since D_{min} is much more sensitive to K in the slow model, it is responsible for the enlarged EG.

IV. DISCUSSION

Our first goal was to obtain general expressions for the rate and curvature dependence of APD and θ that could be used to study any transient or sustained regime of propagation in a 2D disk beyond the period-1 solution analyzed in this paper. We were thus looking for relations that were appropriate for a range of curvature and prematurity as large as possible. Previous works on the paced space-clamped MBR model had shown that the APD dispersion curve was the main determinant of the entrainment response and that it could be accurately represented by an invariant function of the DI.

The ability of the simple iterative model $D_{i+1}=T-A(D_i)$ to reproduce the bifurcation structure of the paced MBR model has clearly established that the DI is more appropriate than the period of stimulation to describe the dynamics [16]. Further works on reentry in a loop have also proven that $A(D)$, complemented by a function $\theta(D)$ that was also invariant, were sufficient to build a low-dimensional model reproducing the main features of the reentry regimes as a function of the radius of the loop [17]. Accordingly, we chose the DI to express the prematurity, and looked for functional representations of APD and θ that, for $K=0$, would be similar to those used for the one-dimensional loop. For θ, these two constraints led us to a representation different from those of previous works in which APD was discarded and the period was used as an independent variable [23,24]. The formulation was usually intended to be applied to regimes of low and moderate curvature [31,32]. The APD restitution curve has to be included in any realistic model of a cardiac excitable cell, since the plateau of the action potential and its sensitivity to prematurity make cardiac cells different from neurons and adapted to the pumping function of the heart.

In $A(K,D)$, the rate and curvature dependence are separated [Eq. (3.5)]. For θ [Eq. (3.4)], K acts both as a scaling factor $[\theta_\infty(K)]$ and as a translation $[f_\theta(D-D_{min})(K)]$ in the rate-dependent part. $\theta_\infty(K)$ is the well known linear approximation that remains surprisingly good, even for K near K_{cr}. f_θ measures how much the prematurity exceeds the local refractory period that is given by $D_{min}(K)$. As intended, these expressions generalize those obtained in the space-clamped and loop configurations for ionic models where the slow memory effects on activation and repolarization are absent.

The functions A and θ were used to investigate the spatial properties of the period-1 solutions. For each $[r_{in}r_{out}]$, the relation linking DI and APD to the speed of propagation and to the period of rotation insures the uniqueness of the solutions. It shows why $A(K,D)$ has to be included in the model. $D_{min}(K)$ is the main determinant of r_{min} in both the normal and slow models. D_{min} limits the maximum curvature that can be reached in period-1 solutions in a range where the influence of K on APD can be neglected. Furthermore, the variation of the DI for each value of r_{in} and r_{out} is minimal, such that the activation and repolarization have the same curvature. This is consistent with the numerical results of [42] with the Luo-Rudy ionic model [43]. In their simulations, the values of APD measured at r_{in} are just slightly above those found at r_{out}. The variation of D_{min} with K is much more important in the slow model, explaining why r_{min} is greater than for the normal model, despite a slower speed of propagation at low DI.

Results for the space-clamped model and the one-dimensional loop show that period-1 responses lose their stability when they reach the DI value for which $dA/dD=1$ [Eq. (3.6)]. The results of Xie *et al.* [42] suggest that a similar criterion could be applied in an annulus. If Eq. (3.6) indeed provides an adequate criterion of stability, it involves

the total derivative of A and can be written as

$$\frac{dA}{dD} = \frac{\partial A}{\partial D} + \frac{\partial A}{\partial K}\frac{dK}{dD}. \tag{4.1}$$

Since the effect of K on APD is minimal for period-1 solutions ($\partial A/\partial K \approx 0$), the criterion of stability for an annulus and ring would be similar.

The period at the critical point, $T_{crit} = D_{crit} + A(D_{crit})$, is thus determined by the characteristics of the restitution curve, and $r_{crit} = \theta(K, D_{crit}) T_{crit}/2\pi$. If D_{crit} is in the flat portion of f_θ, as it is the case in the normal mode, r_{crit} depends only on the curvature and on T_{crit}. For the slow model, the shift of $D_{min}(K)$ is so important that f_θ is not saturated at D_{crit} and f_θ must still be considered in the calculation of r_{crit}. In general, r_{crit} depends on the balance between, on the one hand, the value of D_{crit}, and on the other hand, the slowing of propagation coming from the influence of K on $\theta_\infty(K)$ and $D_{min}(K)$. In our simulations, r_{crit} is slightly greater for the slow model than in the normal model. There is some indication that slowing the gate variable j may stabilize the spiral waves in a continuous 2D medium [44], which is not consistent with what we found for a disk. This may come from differences in the $A(K,D)$, $D_{min}(K)$ and $\theta(K,D)$ functions of the ionic model with which these simulations were done. It may also indicate that the core of the spiral makes a specific contribution that must be included in the low-dimensional model so that it can be applied to a medium without an obstacle [26].

The functions $D_{min}(K)$, $\theta(K,D)$, and $A(K,D)$ were obtained through an approximation, assuming propagation with a constant curvature. The simulations of the simplified model show that, even at $r = r_{min}$, the variation of curvature takes place in two thin regions in the vicinity of r_{in} and r_{out}, K remaining nearly constant everywhere else. This suggests that the functions may indeed provide a good approximation of the dynamics. It also gives some indications of the spatial discretization needed to simulate the ionic model on the annulus. Since the K variation is confined near r_{in} and r_{out}, it suggests using a denser mesh in these regions to avoid a numerical artifact. Results presented by Xie *et al.* [42] show a dependence of the solution on r_{out}, even for a width greater than 1 cm beyond r_{in}. However, they used a mesh with fixed angular width and fixed increment of radius, which gives a coarser spatial resolution as r increases. This may explain the discrepancy between our conclusion and theirs on the influence of r_{out}.

V. CONCLUSION

Varying the obstacle radius changes the period-1 solution. In this regime, K remains low such that the dependence of K on APD can be neglected. The spatial variation of DI also being limited, the same curvature can be assumed for activation and repolarization fronts. However, $A(D)$, $D_{min}(K)$, and $\theta(K,D)$ are necessary for an adequate reconstruction of the solution.

ACKNOWLEDGMENTS

This work was supported by a grant from the Natural Sciences and Engineering Council and the Medical Research Council of Canada.

[1] L.H. Frame, R.L. Page, P.A. Boyden, J.J. Fenoglio, and B.F. Hoffman, Circulation **76**, 1155 (1987).
[2] J. Brugada, L. Boersma, C.J. Kirchhof, V.V. Heynen, and M.A. Allessie, Circulation **84**, 1296 (1991).
[3] T. Ikeda, M. Yashima, T. Uchida, D. Hough, M.C. Fishbein, W.J. Mandel, P.S. Chen, and H.T. Karagueuzian, Circ. Res. **81**, 753 (1997).
[4] M.A. Allessie, F.I. Bonke, and F.J.G. Schopman, Circ. Res. **41**, 9 (1977).
[5] A.M. Pertsov, J.M. Davidenko, R. Salomonsz, W.T. Baxter, and J. Jalife, Circ. Res. **72**, 631 (1993).
[6] M. Okajima, T. Fujimo, T. Kobayshi, and K. Yamada, Circ. Res. **23**, 203 (1968).
[7] V.G. Fast and I.R. Efimov, Physica D **49**, 75 (1991).
[8] L.J. Leon, F.A. Roberge, and A. Vinet, Ann. Biomed. Eng. **22**, 592 (1994).
[9] A. Xu and M.R. Guevara, Chaos **8**, 157 (1998).
[10] D.R. Chialvo and J. Jalife, Nature (London) **330**, 749 (1987).
[11] D.R. Chialvo, R.F. Gilmour, and J. Jalife, Nature (London) **343**, 653 (1987).
[12] A. Vinet, D.R. Chialvo, D.C. Michaels, and J. Jalife, Circ. Res. **67**, 1512 (1990).
[13] D.R. Chialvo, D.C. Michaels, and J. Jalife, Circ. Res. **66**, 525 (1990).
[14] T.J. Lewis and M.R. Guevara, J. Theor. Biol. **146**, 407 (1990).
[15] H. Ito and L. Glass, Physica D **56**, 84 (1991).
[16] A. Vinet and F.A. Roberge, J. Theor. Biol. **170**, 201 (1994).
[17] M. Courtemanche, J.P. Keener, and L. Glass, SIAM (Soc. Ind. Appl. Math.) J. Appl. Math. **56**, 119 (1996).
[18] C. Cabo, A.M. Pertsov, W.T. Baxter, J.M. Davidenko, R.A. Gray, and J. Jalife, Circ. Res. **75**, 1014 (1994).
[19] V.G. Fast and A.G. Kléber, Cardiovasc. Res. **29**, 697 (1995).
[20] S.B. Knisley and B.C. Hill, IEEE Trans. Biomed. Eng. **42**, 957 (1995).
[21] C. Cabo, A.M. Pertsov, J.M. Davidenko, and J. Jalife, Chaos **8**, 116 (1998).
[22] V. S. Zykov, *Simulation of Wave Processes in Excitable Media* (Manchester University Press, Manchester, England, 1987).
[23] V.S. Zykov, Biophysics (USSR) **32**, 365 (1987).
[24] E. Meron and P. Pelcé, Phys. Rev. Lett. **60**, 1880 (1988).
[25] E. Meron, Phys. Rev. Lett. **63**, 684 (1989).
[26] E. Meron, Physica D **49**, 98 (1991).
[27] J.P. Keener, SIAM (Soc. Ind. Appl. Math.) J. Appl. Math. **46**, 1039 (1986).
[28] J.J. Tyson and J.P. Keener, Physica D **29**, 215 (1987).
[29] J.J. Tyson and J.P. Keener, Physica D **32**, 327 (1988).
[30] A.S. Mikhailov and V.S. Zykov, Physica D **52**, 379 (1991).
[31] A.M. Pertsov, M. Wellner, and J. Jalife, Phys. Rev. Lett. **78**, 2656 (1997).
[32] M. Wellner and A.M. Pertsov, Phys. Rev. E **55**, 7656 (1997).

[33] J.-P. Drouhard and F. Roberge, Comput. Biomed. Res. **20**, 333 (1987).
[34] A. Vinet and F.A. Roberge, J. Theor. Biol. **170**, 183 (1994).
[35] A. Vinet and F.A. Roberge, Ann. Biomed. Eng. **22**, 568 (1994).
[36] D. H. Norrie and G. DeVries, *An Introduction to Finite Element Analysis* (Academic Press, New York, 1978).
[37] L.M. Hondeghem and B.G. Katzung, Ann. Rev. Pharmacol. **21**, 387 (1984).
[38] D. P. Zipes and J. J. Jalife, *Cardiac Electrophysiology, From Cell to Bedside* (W. B. Saunders, Philadelphia, 1990), Chap. 92.
[39] J.P. Keener, J. Math. Biol. **29**, 629 (1991).
[40] A. Hagberg and E. Meron, Physica A **249**, 118 (1998).
[41] L.F. Shampine and M.W. Recibelt, SIAM (Soc. Ind. Appl. Math.) J. Comput. **18**, 1 (1997).
[42] F. Xie, Z. Qu, and A. Garfinkel, Phys. Rev. E **58**, 6355 (1998).
[43] C. Luo and Y. Rudy, Circ. Res. **68**, 1501 (1991).
[44] L. J. Leon (unpublished).